Viscoelasticity induces anisotropy in contacts of rough solids

Viscoelastic induced anisotropy in contact mechanics of rough solids

Carmine Putignano*, Nicola Menga, Luciano Afferrante, Giuseppe Carbone

Department of Mechanics, Mathematics and Management,Politecnico di Bari, Bari, Italy.

Abstract

One of most peculiar issues related to soft viscoelastic contacts is the anisotropy induced on the contact solution: when sliding a perfectly isotropic surface over a viscoelastic half-space, the solution in terms of contact areas and displacement distribution is anisotropic. This is due to the different behaviour, in each contact patch, between the leading edge and the trailing one, where the viscoelastic material needs time to relax. Things become even more complicated when the surfaces into contact are already affected by an anisotropic degree, as occurring in many cases due to the manufacturing process. In this paper, by means of a proper Boundary Element Formulation, based on the definition of a viscoelastic periodic Green's function, we carry out, on these topics, a systematic investigation aimed to study the relation between the rigid surface and the deformed half-space anisotropy tensors. In detail, we show that the two tensors are related by means of a linear transformation, based on a rotation and a "stretching" of the roughness anisotropy tensor. The role of anisotropy is, then, studied in relation with the friction force and with the lateral anisotropy induced force originally defined in this study.

Keywords: viscoelasticity, friction, roughness, anisotropy.

1. Introduction

Assessing, by means of analytical, numerical and experimental approaches, what occurs when two solids, with real rough interfaces, come into contact

*Corresponding author. Phone: +39 080 596 2711

Email address: carmine.putignano@poliba.it (Carmine Putignano)

has been, for the last two decades, the focal point of large part of solid mechanics research. There exist different reasons for such an interest in the field. Certainly, on the one hand, the genuinely academic attention addressed to the problem is due to its peculiar intricacy: one of the most fundamental contact mechanics issues deals, indeed, with the presence of the roughness that, given a spectrum covering several orders of magnitude and going down to the atomistic scales, makes extremely complicated the geometrical domain of the problem. However, the vast attention paid to contact mechanics does not finish with its theoretical interest, but it is crucially and strictly related to the practical importance that contact problems have to design and optimize engineering components. Common industrial applications, like tyres, seals and dampers ((1),(2)), are classical examples but a constantly increasing variety of systems, including e.g. bio-adhesive ((4; 5; 6; 7)), cellular scaffolds ((8),(9)) and even touch-screen devices ((10)), requires a better understanding of interfacial phenomena.

The first theoretical answer to these issues has been developed by Greenwood and Williamson in 1966 with the first of the so-called multiasperity theories. Indeed, a variety of models has followed the first pioneering approach (see e.g. (11), (12), (13),(14)): the basic idea, preserved in all the different developments, is to reduce the surface to a discrete distribution of asperities that behave as independent Hertzian punches. Crucially, the mutual interaction between the contact clusters is, thus, neglected: because of such an assumption, multiasperity theories are not able to match experimental outcomes in terms of applied load and contact area ((28)); these models predict an area/load relation that is linear only asymptotically, i.e., for very small, physically meaningless, applied loads (14). Recently, new multiasperity approaches have been proposed to take into account, with a relatevely good accuracy, the elastic coupling and coalescence of asperities (15)(16). In Ref. (17), Persson has developed a totally different approach to the problem: the fundamental point in his theory is related to the contact pressure probability distribution, which is shown to be governed by a diffusive process as we increase the magnification at which the contact interface is observed. Such a theory is exact in full contact conditions, and furnishes approximate, but still qualitatively accurate results for partial contacts. To fill the gap between such qualitative hints and the quantitative predictions required from an application point of view, many numerical methods and, in particular, several Boundary Element approaches, developed either in the real ((18),(19),(20),(21),(22),(23)) and in the Fourier space ((26),(27),(24),(25)),

have been proposed. These techniques have nowadays reached an extremely high level of accuracy , but are, at the same time, in most cases affected by a significant limitation: they have been implemented for linearly elastic contacting solids.

However, there exists a wide number of cases and, specifically, all those involving soft materials, where a clear non-elastic time-dependent mechanical behaviour is exhibited. Soft matter, which marks a variety of systems, ranging from civil engineering ((2),(3)) to biomechanics ((8),(9),(29)), can be described, with good approximation, by a linearly viscoelastic rheology. Recently, given the theoretical and practical importance of viscoelastic contact mechanics, intense research activities have been dedicated to the theme ((30),(31),(33),(34),(35),(36),(37),(38),(40)) : different conditions , including constant sliding velocity, reciprocating motion and lubricated contacts, have been explored by some of the authors of this paper and other research groups in the word ((30),(31),(33),(34),(35),(36),(37),(38),(40), (41),(42), (43), (49),(48)). Despite there are still many issues to enlighten, these studies have already shown how deeply viscoelasticity affects the contact solution in terms of contact area, separation, stiffness and, ultimately, friction. Results can differ orders of magnitude from purely elastic conditions. In this paper, we systematically focus on an issue that, so far, has not been properly investigated, but has a dramatic theoretical and practical significance. This is the anisotropy induced on the contact solution by the material viscoelastic rheology: as shown in Ref. (37), when a rigid isotropic surface slides over a viscoelastic layer, the contact solution shows a strong anisotropy in the distribution of both contact clusters and displacement. This is due to the different behaviour, in each contact area, between the leading edge and the trailing edge, where the material needs time to relax. Things become even more complicated when the surface in contact with the viscoelastic layer is already anisotropic, as often occurring in real interfaces due to the manufacturing treatment. In addition to its theoretical importance, the practical implications of the viscoelastic induced anisotropy are dramatic. As an example, let us focus on the sealing components and, thus, on the percolation phenomenon: most of the model and theories in the field ((52),(51),(50),(53)) assume that the distribution of the contact patches is perfectly isotropic. Actually, in the case of viscoelastic interfaces, the contact regions are anisotropic and this entails, for the percolating fluid, preferential channels, which are totally ignored when considering a purely elastic model. As a consequence, current model can underestimate the percolating flow in rubber-based vis-

coelastic seals.

In this paper, an extensive study of the viscoelastic induced anisotropy is presented and, specifically, anisotropy of the deformed half-space and implications on global contact area, separation and friction are analyzed. Furthermore, the occurrence of a lateral constrain force is shown to be due to a combination between the anisotropy of the contacting surface and the layer viscoelasticity. All the calculations are carried out by means of a Boundary Element methodology, based on the formulation given in Ref. (31) , but properly modified to impose periodic conditions to the domain. This enables us to eliminate any influence related to finite size effects. We conclude the paper with some final remarks about the importance of taking into account the proper rheology of the contacting solids and, thus, the anisotropy of the solution.

2. Mathematical Formulation

In Ref. (31), for a rigid indenter in sliding contact with a linear viscoelastic slab, it is shown that the translational invariance and the elastic-viscoelastic correspondence principle (44) can be employed to obtain the following integral equation that correlates the surface displacement $u(\mathbf{x},t)$ and the Lagrangian time derivative $\dot{\sigma}(\mathbf{x},t)$ of the normal interfacial stress $\sigma(\mathbf{x},t)$:

$$u(\mathbf{x},t)=\int_{-\infty}^{t}d\tau\int d^{2}x'\,\mathcal{J}(t-\tau)\,\mathcal{G}(\mathbf{x}-\mathbf{x}')\,\dot{\sigma}(\mathbf{x}',\tau)\,. \tag{1}$$

We observe that both the distributions, $u(\mathbf{x},t)$ and $\dot{\sigma}(\mathbf{x},t)$, are clearly dependent on the in-plane position vector $\mathbf{x}$ and on the time parameter t. Furthermore, in Eq. (1), $\mathcal{G}(\mathbf{x})$ and $\mathcal{J}(t)$ are the elastic Green's function and the creep function. As well known in linear viscoelasticity, $\mathcal{J}(t)$ has to satisfy causality, i.e. $\mathcal{J}(t<0)=0$, and, for a generic linear viscoelastic material (44), can be expressed as $\mathcal{J}(t)=\mathcal{H}(t)\left[1/E_0-\int_0^{+\infty}d\tau\mathcal{C}(\tau)\exp(-t/\tau)\right]$, where $\mathcal{H}(t)$ is the Heaviside step function, E_0 is the low-frequency elastic modulus, $\mathcal{C}(\tau)$ is a strictly positive function usually defined as the creep (or retardation) spectrum (44; 45), and τ is the relaxation time, continuously distributed on the real axis.

Now, the direct solution of Eq. (1) requires to discretize both the time and the space domains, thus resulting computationally high demanding (36)(38)(39)

. This is particularly critical for rough interfaces, where, because of the large width of the rough spectrum, we have a huge number of time and space scales involved in the process and, thus, we cannot solve the problem with the computational resources currently available. However, if we focus our attention on the case of a rough punch sliding, at constant velocity, over a viscoelastic half-space and we neglect any thermal effect, given the steady-state features of the system, it is possible to simplify Eq. (1) as:

$$u\left(\mathbf{x}\right)=\int d^{2}x'G\left(\mathbf{x}-\mathbf{x}',\mathbf{v}\right)\sigma\left(\mathbf{x}'\right) \tag{2}$$

where $G\left(\mathbf{x}-\mathbf{x}',\mathbf{v}\right)$ depends only parametrically on the speed. Passing from Eq. (1) to Eq. (2) is crucial since it enables us to exploit the steady-state conditions of the system and, specifically, to discretize only the space domain. In Ref. (31), a specific mathematical procedure has been developed to determine $G\left(\mathbf{x},\mathbf{v}\right)$. However, let us follow here a different approach since we want to explicitly impose periodic conditions to the system by replacing $G\left(\mathbf{x},\mathbf{v}\right)$ with a proper periodic Green's function $G_{\lambda}\left(\mathbf{x},\mathbf{v}\right)$ (32).

To this aim, it is convenient to move to the Fourier space. Thus, let us take the Fourier-transform of Eq. (1):

$$u\left(\mathbf{q}\right)=M_{zz}\left(\mathbf{q},\mathbf{q}\cdot\mathbf{v}\right)\sigma\left(\mathbf{q}\right) \tag{3}$$

where $M_{zz}\left(\mathbf{q},\mathbf{q}\cdot\mathbf{v}\right)$ depends on the conditions of the linear viscoelastic solid and can be written generally as:

$$M_{zz}\left(\mathbf{q},\mathbf{q}\cdot\mathbf{v}\right)=-\frac{2\left(1-\nu^{2}\right)}{E\left(\mathbf{q}\cdot\mathbf{v}\right)}\frac{1}{\mathbf{q}}S(\mathbf{q}) \tag{4}$$

with $E\left(\mathbf{q}\cdot\mathbf{v}\right)$ and $S(\mathbf{q})$ being respectively the viscoelastic complex modulus -related to the Fourier transformed creep function $\mathcal{J}\left(\omega\right)$ by means of the relation $E\left(\omega\right)=\left[i\omega J\left(\omega\right)\right]^{-1}$ - and a correcting factor that accounts for the boundary conditions imposed on the viscoelastic layer and is equal to $S(\mathbf{q})=1$. Now, in order to find $G_{\lambda}\left(\mathbf{x},\mathbf{v}\right)$, let us load the system with a distribution $\chi_{\lambda}\left(\mathbf{x}\right)$ of uniform pressures, each acting on a square with side a and periodically applied with a spatial periodicity λ. This will be, later, useful when solving the integral relation between $u\left(\mathbf{x}\right)$ and $\sigma\left(\mathbf{x}\right)$ by discretizing the contact domain with boundary elements. For time being, let us formulate the distribution χ_{λ}:

$$\chi_\lambda(x,y) = \sum_{k,h=-\infty}^{+\infty} \chi_a\left(\mathbf{x} - \frac{2\pi}{\lambda}\mathbf{k}\right) \tag{5}$$

where χ_a is a pressure distribution being constant in the loaded square and equal to zero outside and $\mathbf{k}$ is the vector $\mathbf{k} = (k,h)$. Now, if we load the system with χ_λ, we obtain in the real space:

$$G_\lambda(\mathbf{x},\mathbf{v}) = \int d^2x' G(\mathbf{x}-\mathbf{x}',\mathbf{v})\,\chi_\lambda(\mathbf{x}'), \tag{6}$$

and in the Fourier space:

$$M_\lambda(\mathbf{q},\mathbf{q}\cdot\mathbf{v}) = M_{zz}(\mathbf{q},\mathbf{q}\cdot\mathbf{v})\,\chi_\lambda(\mathbf{q}). \tag{7}$$

Let us focus on this second expression. We can easily find the Fourier transform $\chi_\lambda(\mathbf{q}) = \int d^2x \chi_\lambda(\mathbf{x})\, e^{-i\mathbf{q}\cdot\mathbf{x}}$ as:

$$\chi_\lambda(\mathbf{q}) = \sum_{k,h=-\infty}^{+\infty} \frac{4\sin\left(\frac{1}{2}\mathbf{q}_{hk}a\right)}{khq_0^2}\delta\left(\frac{\mathbf{q}}{q_0} - \mathbf{k}\right) \tag{8}$$

with the wavevector $\mathbf{q}_{hk} = (hq_0, kq_0)$. Now, we can obtain $G_\lambda(\mathbf{x},\mathbf{v})$ as inverse Fourier transform of $M_\lambda(\mathbf{q},\mathbf{q}\cdot\mathbf{v})$ as $G_\lambda(\mathbf{x},\mathbf{v}) = (1/4\pi^2)\int M_\lambda(\mathbf{q},\mathbf{q}\cdot\mathbf{v})\, e^{i\mathbf{q}\cdot\mathbf{x}}$. By discretizing such an expression, we can rewrite $G_\lambda(\mathbf{x},\mathbf{v})$:

$$G_\lambda(\mathbf{x},\mathbf{v}) = \left(\frac{q_0}{2\pi}\right)^2 \sum_{k,h=-\infty}^{+\infty} M_{zz}(\mathbf{q}_{hk}, \mathbf{q}_{hk}\cdot\mathbf{v})\,\frac{4\sin\left(\frac{1}{2}\mathbf{q}_{hk}a\right)}{khq_0^2} e^{i\mathbf{q}_{hk}\cdot\mathbf{x}} \tag{9}$$

Eq. (9) shows that $G_\lambda(\mathbf{x},\mathbf{v})$ is equal to a Fourier series and can be computed very rapidly by means of the Inverse Fast Fourier Transform algorithm.

Now, we can proceed to the numerical solution of the contact problem. The contact area can be meshed in M square cells: in each j-th elementary area with a side a_j, the normal stress σ will be constant and equal to σ_j. The displacement is, on its turn, measured at the centre $\mathbf{x}_i$ of each i-th square and is equal to $u_i = u(\mathbf{x}_i, t)$. Thus, we can write:

$$u_i = \sum_{j=1}^{M} G_\lambda(\mathbf{x}_i - \mathbf{x}_j, \mathbf{v})\,\sigma_j a_j^2 \tag{10}$$

At this point, the contact problem, reduced to a linear system, can be solved by employing the iterative technique developed in Ref. (19) for elastic contacts. We observe that such a numerical procedure has a unique advantange: the formulation is fully periodic since it employs the periodic Green's function $G_\lambda(\mathbf{x}, \mathbf{v})$, and, at the same time, calculations are carried out in the real domain, without having any aliasing problem. Indeed, such an issue could arise when the formulation is made periodic by directly transforming Eq. (2) in the Fourier space.

Then, once the contact solution has been determined in terms of contact areas, stresses and strains, it is possible to focus on the frictional force F_T tangentially generated at the contact interface. Incidentally, let us recall that, unlike the Coulomb friction, the viscoelastic friction is not related to the interfacial interaction between the contacting bodies, but to the internal hysteretic dissipation in the solid (31). Now, in the case of isotropic punches in contact with the viscoelastic half-space, there exists just a component which opposes the motion and is the so-called viscoelastic friction force. When dealing with anisotropic surfaces, as in this paper, things become more complicated. Indeed, without any loss of generality, let us assume that the velocity $\mathbf{v}$ is equal to $\mathbf{v} = v\mathbf{i}$, where $\mathbf{i}$ is the unit vector of the x-axis. The viscoelastic interfacial tangential force still has, as usually shown in Ref. (31), the viscoelastic friction component F_x:

$$F_x = \int_D d^2x \sigma(\mathbf{x}) \frac{\partial u}{\partial x} \tag{11}$$

The viscoelastic contact coefficient is, then, defined as $f = F_x/F_n$ with F_n being the normal force applied to the contact interface. However, in the case of anisotropic surfaces, we have also a lateral force F_y:

$$F_y = \int_D d^2x \sigma(\mathbf{x}) \frac{\partial u}{\partial y} \tag{12}$$

A detailed discussion of the two components F_x and F_y is reported in Appendix A, but let us point out here that, although F_y does not carry out any work, it has to be present to guarantee the global equilibrium of the system.

3. Results and discussion

In this paper, our aim is to understand what happens when sliding an anisotropic surface over a viscoelastic half-space. To this end, in our cal-

culations, following the procedure described in detail in Appendix B, we generate several surfaces with a different degree of anisotropy: indeed, in order to quantify such an anisotropy, let us focus on the surface power spectral density $C(\mathbf{q})$ that is equal to $C(\mathbf{q}) = (2\pi)^{-2} \int d^2x \langle h(\mathbf{0}) h(\mathbf{x}) \rangle \exp(-i\mathbf{q} \cdot \mathbf{x})$ with $h(\mathbf{x})$ being the height distribution and with the symbol $\langle \cdot \rangle$ standing for the ensemble average. In the case of anisotropic surface, $C(\mathbf{q})$ is elliptical: in our work, we produce surfaces with different ε, defined as the eccentricity of $C(\mathbf{q})$, and with different values of the angle α, that is, the angle between the major axis of the elliptical $C(\mathbf{q})$ and the direction of the x-axis. Given the afore-mentioned assumption on $\mathbf{v}$, the latter coincides with the velocity direction. In detail, we generate two sets of surfaces: one with $\alpha = 0$ and $\varepsilon = 1$, 0.8 , 0.6 , 0.4 , 0.2 and the other one with $\varepsilon = 0.6$ and $\alpha = 0$, $\pi/8$, $\pi/4$, $3/8\pi$, $\pi/2$. All these surfaces have spectral components in the range $q_r < q < q_c$, where $q_r = 2\pi/L_0$, with L_0 being the side of the square punch equal to $L_0 = 0.01$ m, $q_r = Nq_0$ and N number of scales (or wavelengths).

Calculations are obtained with $N = 64$. Furthermore, with regards to the material properties, in our calculations, we use a one relaxation time material with a high frequency modulus E_∞ equal to $E_\infty = 10^8$ Pa, the ratio $E_\infty/E_0 = 11$ and the Poisson ratio being $\nu = 0.5$.

Figure 1 emphasizes an effect enlightened for the first time in Ref. (41). Basically, when sliding a perfectly isotropic rough surface over a linearly viscoelastic solid, the solution in terms of contact clusters results anisotropic: specifically, each contact area tends to shrink at the contact trailing edge, where the material needs time to relax. As a consequence, each contact cluster results stretched perpendicularly to the velocity.

Such an effect can be quantified by defining, in a certain range of wave vectors $\zeta_1 q_0 < |\mathbf{q}| < \zeta_2 q_0$, the symmetric anisotropy tensor of the deformed surface $\mathcal{M}(\zeta_1, \zeta_2)$:

$$\mathcal{M}(\zeta_1, \zeta_2) = \int_{\zeta_1 q_0 < |\mathbf{q}| < \zeta_2 q_0} d^2q \mathbf{q} \otimes \mathbf{q} C_d(\mathbf{q}, \zeta_1, \zeta_2) \tag{13}$$

where $C_d(\mathbf{q}; \zeta_1, \zeta_2) = (2\pi)^{-2} \int d^2x \langle u(\mathbf{0}; \zeta_1, \zeta_2) u(\mathbf{x}; \zeta_1, \zeta_2) \rangle \exp(-i\mathbf{q} \cdot \mathbf{x})$ is the power spectral density of the filtered deformed surface $u(\mathbf{x}; \zeta_1, \zeta_2)$. We notice that C_d could have been divided for $|\mathbf{q}|^2$ so that, also in the case of large range $[\zeta_1, \zeta_2]$, the dominant contribution of large wavevectors would have resulted compensated. However, since the surfaces employed in this

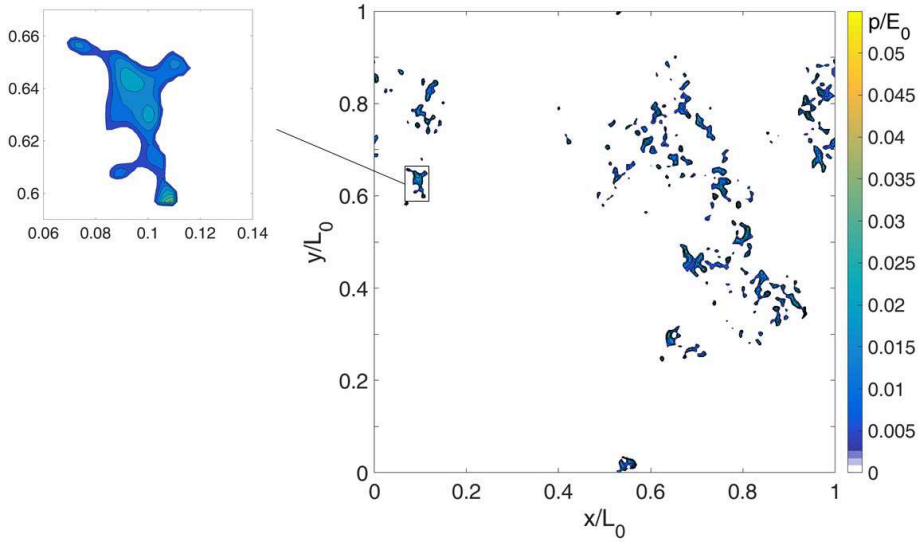

Figure 1: Contact area for a perfectly isotropic surface (eccentricity parameter ε equal to $\varepsilon = 1$) sliding over a linearly viscoelastic layer. In the inset, we zoom on single patch of the contact area.

study have a spectral component in a relatively small range, we prefer to employ the original form in Equation (10) to preserve the relation, as later explained, between the components of $\mathcal{M}$ and the geometrical moments of the deformed layer. At the same time, we notice that the band-pass filter in the interval $[\zeta_1, \zeta_2]$ can allow us to focus on the frequencies where the viscoelastic effects are higher.

Now, with regards to $\mathcal{M}$, let us observe that the quantity $\mathcal{M}_{ij} = \int_{\zeta_1 q_0 < |\mathbf{q}| < \zeta_2 q_0} d^2 q q_i q_j C_d(q)$, with i and $j = 1, 2$, is the second order moments of the power spectral density of the filtered surface, i.e. $\mathcal{M}_{11} = \mu_{20} = \langle u_x^2 \rangle$, $\mathcal{M}_{22} = \mu_{02} = \langle u_y^2 \rangle$, $\mathcal{M}_{12} = \mu_{11} = \langle u_x u_y \rangle$, where $u_x = \partial u / \partial x$, $u_y = \partial u / \partial y$ (see also Ref. (47)). It is useful to define, moving from the symmetric tensor $\mathcal{M}$, the quadratic form $\mathcal{Q}(\mathbf{x}) = \mathcal{M}_{ij} x_i x_j$; thus, in a polar reference system with $x = r\cos\theta$, and $y = r\sin\theta$, one easily obtains:

$$\mathcal{Q}(\mathbf{x}) = r^2 \left| \nabla u \cdot \mathbf{e}(\theta) \right|^2 = r^2 \mu_2(\theta)$$

where $\mathbf{e}(\theta)$ is the unit vector $(\cos\theta, \sin\theta)$ and

$$\mu_2(\theta) = \mu_{20}\cos^2(\theta) + 2\mu_{11}\sin(\theta)\cos(\theta) + \mu_{02}\sin^2(\theta) \tag{14}$$

is, then, the average square slope for the profile obtained by cutting the deformed surface $u(\mathbf{x};\zeta_1,\zeta_2)$ along the direction θ (37). If we look at the quantity $\mu_2(\theta)$ in a polar diagram, we observe that, if we have isotropy, $\mu_2(\theta)$ is circular; otherwise, we have a different shape. At a quantitative level, the degree of anisotropy can be quantified by means of the ratio $\gamma_d = \mu_{2\,\min}/\mu_{2\,\max}$ between the minimum $\mu_{2\,\min}$ and the maximum $\mu_{2\,\max}$ eigenvalues of the tensor $\mathcal{M}$, and the principal direction of anisotropy through the eigenvectors of the tensor $\mathcal{M}$, e.g. by the value of the angle θ_d maximizing $\mu_2(\theta)$, i.e. $\mu_2(\theta_d) = \mu_{2\,\max}$.

In a perfectly similar way, it is possible to define the anisotropy tensor $\mathbf{M}$ for the rough surface as $\mathbf{M}(\zeta_1,\zeta_2) = \int_{\zeta_1 q_0<|\mathbf{q}|<\zeta_2 q_0} d^2q\mathbf{q}\otimes\mathbf{q}C(\mathbf{q},\zeta_1,\zeta_2)$: its components are ,then, $M_{11} = m_{20} = \langle h_x^2\rangle$, $M_{22} = m_{20} = \langle h_y^2\rangle$, $M_{12} = m_{11} = \langle h_x h_y\rangle$ with $h_x = \partial h/\partial x$ and $h_y = \partial h/\partial y$. For the roughness anisotropy tensor $\mathbf{M}$, we can define its quadratic form Q, and, finally, the parameters γ_s and θ_s for the quantity $m_2(\theta)$, that is, the average square slope for the profile obtained on the rough surface $h(\mathbf{x};\zeta_1,\zeta_2)$ along the direction θ (37). Incidentally, we notice that θ_s must be equal to the anisotropy angle α. Furthermore, we observe that all the surfaces employed in this study have been generated by keeping constant the trace of the anisotropy tensor $\mathbf{M}$: the quantity $t = m_{20} + m_{02}$ is equal to $t = 6.25\cdot 10^{-4}$.

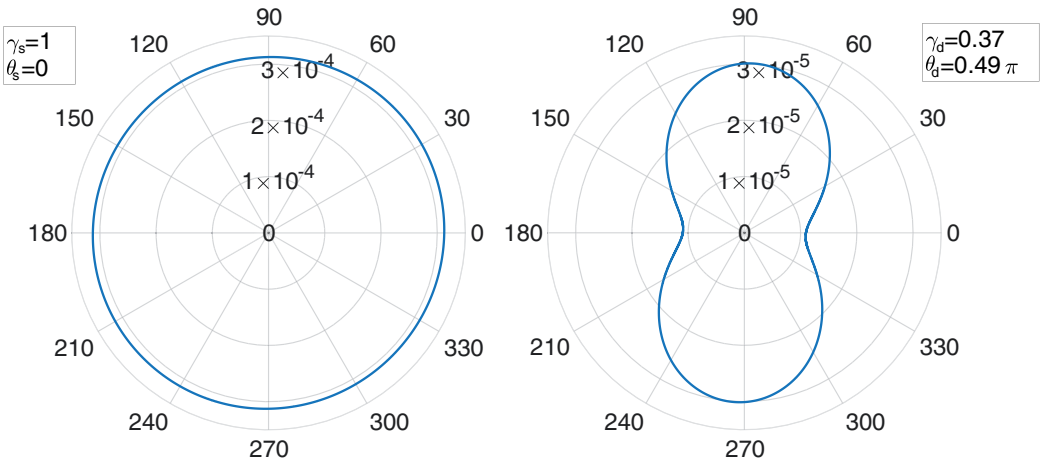

Figure 2: Polar plots of $m_2(\theta)$ for the rigid surface (*on the left*) and $\mu_2(\theta)$ for the deformed half-space (*on the right*), for a dimensionless speed equal to $v\tau/L_0 = 0.13$ and a constant normal pressure p equal to $p = 32$ kPa.

Coming back to the case of the isotropic surface in contact with a viscoelastic half-space in Figure 1, we can represent $m_2(\theta)$ and $\mu_2(\theta)$. Indeed, Figure 2 contains the polar plots for both quantities: as expected, $m_2(\theta)$ is perfectly circular (with $\gamma_s = 1$), whereas $\mu_2(\theta)$ is elliptical with $\gamma_d = 0.37$ and θ_d is approximately $\pi/2$. This is perfectly consistent with what observed in Figure 1: the contact regions result stretched perpendicularly to the velocity direction and the angle of maximum anisotropy has to be close to $\pi/2$. Indeed, as shown in Ref. (31), the contact area shrinkage and the anisotropic shape for the spectral moment $\mu_2(\theta)$ are strictly correlated: the contraction of each contact cluster at the trailing edge implies, in practise, a high-pass filter applied to the frequencies corresponding to the scales along the velocity direction. Consequently, the spectral moment of the deformed profile has to reduce in such a direction. This is, indeed, what is observed in Figure 2.

Now, when dealing with anisotropic surfaces, if we assume pure normal indentation conditions, the spectral moment of the deformed layer $\mu_2(\theta)$ will be consistent with the spectral moment of the surface $m_2(\theta)$ as the system will relax and reach a rubbery elastic status. Specifically, the principal directions for $\mu_2(\theta)$ and $m_2(\theta)$ will correspond. Now, if the anisotropic surfaces starts to slide over the viscoelastic layer, contact areas tend to shrink at the trailing edge along the velocity direction and, thus, when looking at the deformed surfaces, the high-pass filter mentioned before applies to the scales along the speed direction. This effect, clearly, combines with $m_2(\theta)$ of the anisotropic surface. The contact solution will be characterized by an anisotropic distribution that will be different from the surface initial anisotropy, but, at the same time, will not be governed, simply and exclusively, as for the sliding contact of an isotropic surface, by the motion velocity.

All this is clear in Figure 3, where, fixed the eccentricity $\varepsilon = 0.6$ and the velocity direction, being coincident with the x-axis, we study how the system evolves with the variation of the anisotropy angle α. Specifically, we plot $m_2(\theta)$ and $\mu_2(\theta)$ in order to appreciate the role carried out by the viscoelasticity. Our analysis starts with an angle α equal to 0, i.e., with a surface whose main anisotropy direction is along the velocity $\mathbf{v}$. Under such a condition, since viscoelasticity tends to stretch the contact clusters perpendicularly to $\mathbf{v}$, ultimately, the system tends to be regularized as the isotropy of the contact solution is increased. Conversely, by rotating the surface and, then, by increasing the angle α, the anisotropy induced by the viscoelastic rheology is progressively concordant with the surface anisotropy;

as a result, the contact solution anisotropy grows. The crucial point is that, because of the viscoelastic rheology of the solid into contact, and depending on the relative angle between the velocity direction and the surface main anisotropy direction, the anisotropy characteristics of the contact solution are strongly modified.

All this can be defined on a more quantitative basis by determining in detail the algebraic operations carried out on $\mathbf{M}$ to get $\mathcal{M}$. To this aim, let us introduce the stretch tensor being defined in our cartesian reference system as:

$$\mathbf{\Sigma} \equiv \begin{bmatrix} \sigma_1 & 0 \\ 0 & \sigma_2 \end{bmatrix} \tag{15}$$

We can rotate $\mathbf{\Sigma}$ at the anisotropy angle α by applying the rotation matrix $\mathbf{R}_\alpha$: thus, we obtain $\mathbf{\Sigma}_d = \mathbf{R}_\alpha \mathbf{\Sigma} {\mathbf{R}_\alpha}^T$. We can, then, write $\mathcal{M}$ as:

$$\mathcal{M} = \mathbf{R}_\varphi \mathbf{\Sigma}_d \mathbf{M} \mathbf{R}_\varphi^{\mathbf{T}} \tag{16}$$

where $\mathbf{R}_\varphi$ is the rotation matrix associated to the angle $\varphi = \theta_d - \theta_s = \theta_d - \alpha$. Basically, $\mathcal{M}$ can be obtained by "stretching" the surface anisotropy tensor $\mathbf{M}$ and, then, by carrying a rotation at the angle φ . Eq. (16) can be easily proved. Let us observe that, if α is the surface anisotropy angle and $\mathbf{R}_\alpha$ is the associated rotation matrix, $\mathbf{M}$ can be diagonalized by carrying out a rotation at an angle $-\alpha$ and by remembering that $\mathbf{R}_\alpha = \mathbf{R}_\alpha^T$: we obtain, as a result, $\mathbf{M}_d = \mathbf{R}_\alpha^T \mathbf{M} \mathbf{R}_\alpha$. Due to the viscoelasticity, $\mathbf{M}_d$ is then stretched with $\mathbf{\Sigma}$ and rotated back to its original position: we get, thus, $\mathbf{R}_\alpha \mathbf{\Sigma} {\mathbf{R}_\alpha}^{\mathbf{T}} \mathbf{M}$. The latter has to be finally rotated at the angle φ to retrieve $\mathcal{M} = \mathbf{R}_\varphi \mathbf{R}_\alpha \mathbf{\Sigma} {\mathbf{R}_\alpha}^{\mathbf{T}} \mathbf{M} \mathbf{R}_\varphi^T = \mathbf{R}_\varphi \mathbf{\Sigma}_d \mathbf{M} \mathbf{R}_\varphi^T$.

The crucial point here is that, in order to define the transformation carried out on $\mathbf{M}$, it is necessary to determine just three parameters, that is, σ_1 , σ_2 and φ, being functions of the viscoelastic material properties, of the velocity, of the normal load and, interestingly, of the relative angle between the velocity direction and the surface main anisotropy one. Indeed, when this angle is equal to $\pi/2$, φ reaches its maximum, while it tends to vanish when the velocity and the surface anisotropy directions coincide. Incidentally, we observe that, in the elastic limits, φ must be zero, and σ_1 and σ_2 have to be equal. Let us observe that such a strict relation between $\mathbf{M}$ and $\mathcal{M}$ has indeed a dramatic importance in a variety of systems: as an example, we recall the percolation problems, where, own to the anisotropic contact

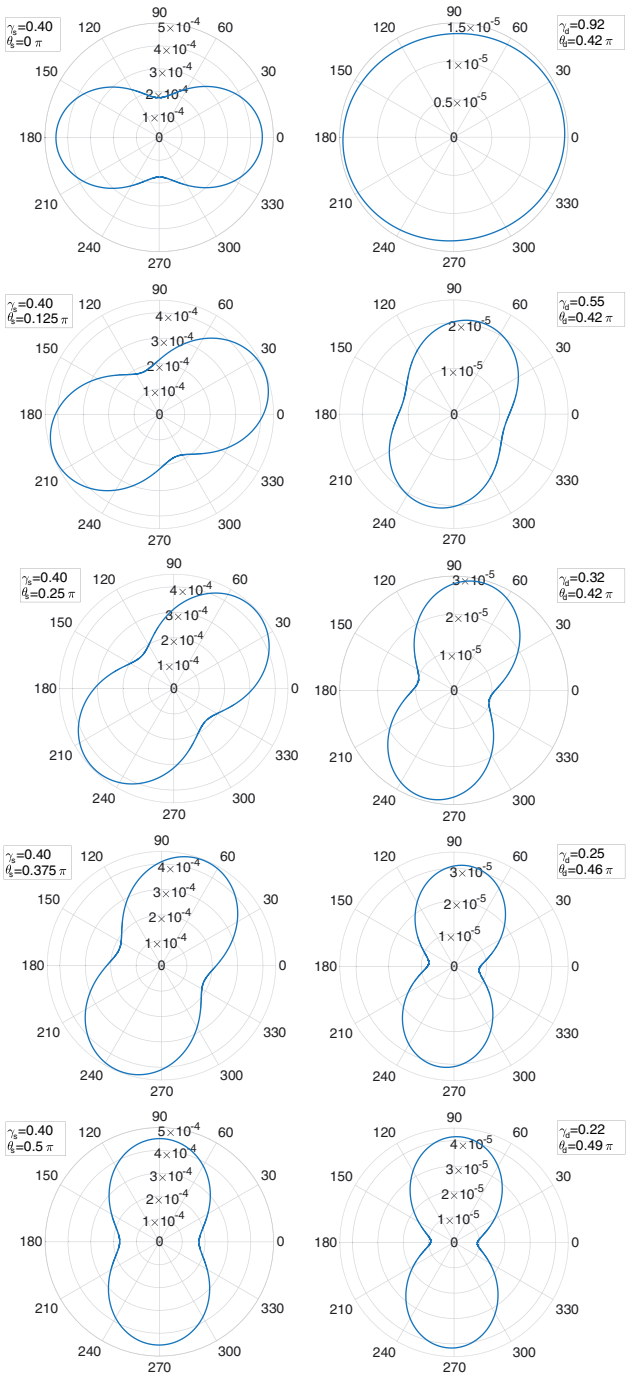

Figure 3: Polar plots of $m_2(\theta)$ for the rigid surface (*on the left*) and $\mu_2(\theta)$ for the deformed half-space (*on the right*), for a dimensionless speed equal to $v\tau/L_0 = 0.13$ and a constant normal pressure p equal to $p = 32$ kPa.

clusters distribution, leaking flow can find preferential channels to percolate. As a consequence, the percolation threshold tends to decrease with a marked increment of the system permeability. For such a reason, it is crucial to determine σ_1 , σ_2 and φ so that $\mathcal{M}$ is known as a rotation and a stretch of $\mathbf{M}$.

In Figure 4, we observe that the effects of the surface anisotropy angle on global quantities, like contact area and separation, may be less evident. This can be explained easily by observing that, in the elastic limits, i.e. when the sliding speed is very low or very high, nothing can change by rotating the surface, i.e. by changing the anisotropy angle. Consistently, in the intermediate speed, we cannot expect a large dependence on the anisotropy angle. In detail, as for the contact area A/A_0, such a quantity slightly increases with α: a minimum is, indeed, reached for $\alpha = 0$. From a physical point of view, this can be explained observing that, for $\alpha = 0$, the majority of the scales are along the velocity direction, i.e., along the direction where the contact patches undergo a shrinkage at the contact trailing edge. Basically, this is equivalent to a stiffening of the contact interface and, thus, a reduction of the contact area in comparison with what occurs with larger angles α. Coherently, when looking at the dimensionless separation s/h_{rms}, in the proper viscoelastic range, that is, between the low and the high frequency elastic regimes, such a quantity decreases with α: a larger separation occurs when the contact area is smaller, that is, for smaller angles α. Incidentally, as expected when dealing with the mean separation in rough contacts (19), we observe that s/h_{rms} is also affected by the different maximum heights of each realization numerically generated for the rough surfaces. This explains why, at high speed, i.e. in the glassy elastic regime, where the separation is largest, the curves referring to different values of α converge to slightly different values.

Now, let us finally focus on the viscoelastic friction since the combination of the surface anisotropy with the material viscoelasticity has significant implications on the energy dissipated by the viscoelastic layer. In Figure 5, we plot the viscoelastic friction f as a function of the velocity for different values of angle α. What we observe is that, for a fixed value of the velocity, the friction decreases when increasing the angle α and, specifically, reaches its minimum when the velocity is perpendicular to the main anisotropy direction, that is, for α being equal to $\alpha = \pi/2$. In fact, by increasing α, we decrease the spectral moment in the velocity direction, being equal to m_{20}: this means that, along the sliding direction, there are less scales capable of

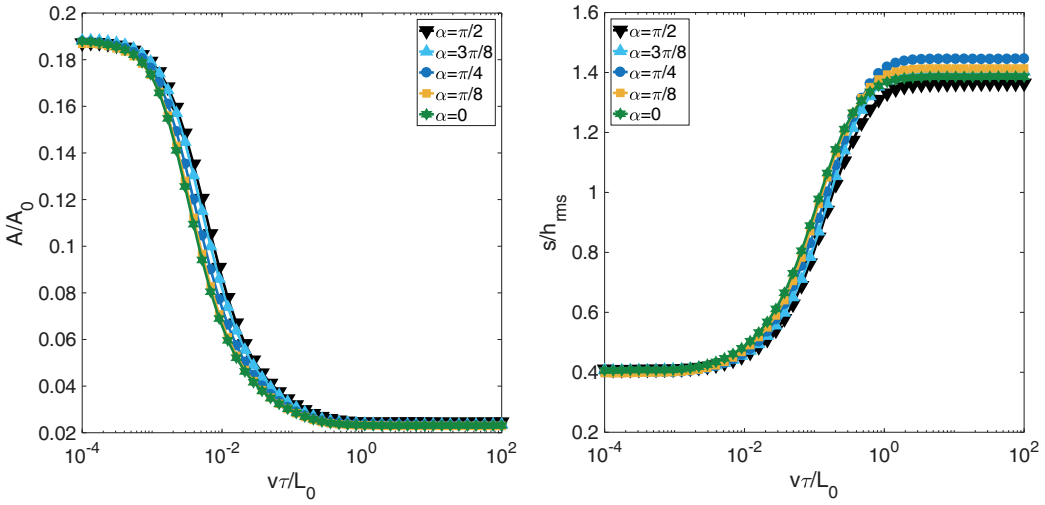

Figure 4: Contact area A/A_0 (*on the left*) and separation s/h_{rms} (*on the right*) as a function of the dimensionless speed equal to $v\tau/L_0$ for a constant normal pressure p equal to $p = 32$ kPa.

dissipating energy. Thus, the viscoelastic friction must decrease. Such an effect, related to the spectral moment $m_2(\theta)$ and to the number of scales in the speed direction is confirmed in Figure 6 , where, fixed $\alpha = 0$, we change the eccentricity ε. Specifically, we pass from a perfectly isotropic surface with $\varepsilon = 1$ to a strongly anisotropic surface by keeping again constant anisotropy tensor trace t. As a consequence, by decreasing ε, we decrease $m_2(\theta)$ in the velocity direction and, thus, reduce the quantity of dissipating scales and the overall friction.

Coming back to the role of the anisotropy angle α, as mentioned before, one of the most interesting issues when focusing on viscoelastic contacts of anisotropic surfaces deals with the lateral force occurring in the system. This force does not carry out any work, but it is essential, as a constrain force, to guarantee the system equilibrium. Indeed, from a physical point of view, in the case of viscoelastic contacts, the pressure distribution is dissymmetric and, to have the global equilibrium, has to be compensated by tangential stresses: these have one component in the sliding direction, which dissipates energy and produces the viscoelastic friction, and the other one, which is the viscoelastic later force. By recalling that, without any loss of generality, we have assumed $\mathbf{v} = v\mathbf{i}$ the two components have been defined respectively

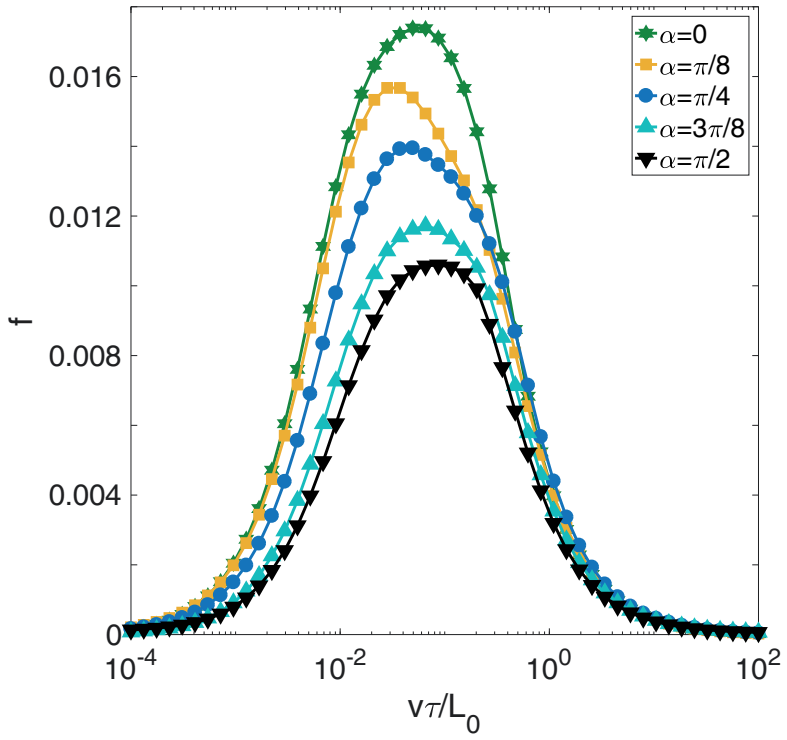

Figure 5: Viscoelastic friction coefficient $f = F_x/F_n$ as a function of the dimensionless speed equal to $v\tau/L_0$ for a constant normal pressure p equal to $p = 32$ kPa and for different values of the anisotropy angle α.

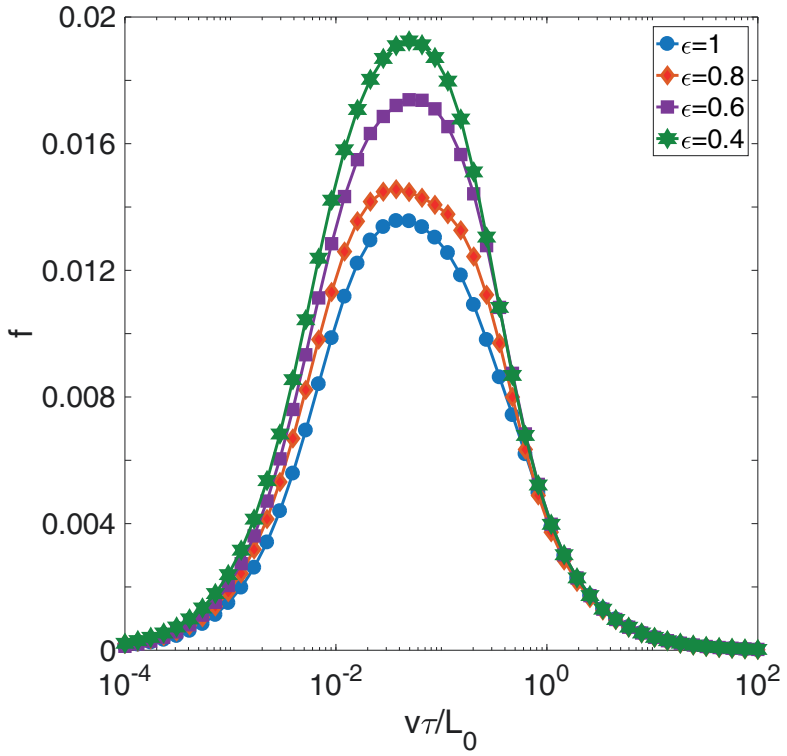

Figure 6: Viscoelastic friction coefficient $f = F_x/F_n$ as a function of the dimensionless speed equal to $v\tau/L_0$ for a constant normal pressure p equal to $p = 32$ kPa and for different values of the anisotropy angle ε.

as F_x and F_y .The latter occurs, then, if the pressure distribution is dissymmetric also with respect to the y-axis: clearly, this cannot happen if the velocity direction coincides with one of the principal directions of the surface anisotropy spectrum. Indeed, what we see in Figure 7 is that the lateral force vanishes for α being equal to 0 and $\pi/2$. Conversely, there exists F_y for different values of α: although it is smaller than F_x, it has a theoretical significance and, in practical applications, can be important when contact forces become large.

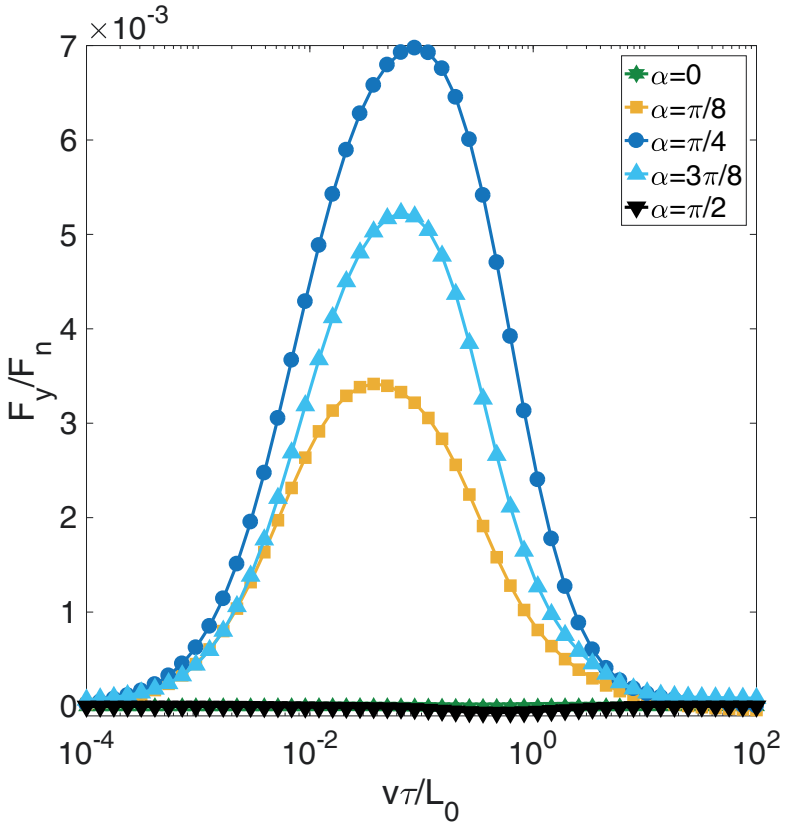

Figure 7: Dimensionless lateral force F_y/F_n as a function of the dimensionless speed equal to $v\tau/L_0$ for a constant normal pressure p equal to $p = 32$ kPa.

4. Conclusion

In this paper, we focus on the anisotropy that is induced, in the case of a viscoelastic rheology, on the contact mechanics between rough solids. More specifically, a detailed investigation is carried out to understand how the viscoelasticity induced anisotropy of the contact solution is related to the anisotropy degree of the rigid surface into contact with the viscoelastic half-space. Such a study is implemented by means of an original Boundary Element formulation, where the Green's function is properly defined in the Fourier space and, then, obtained in the real space by applying the Inverse Fast Fourier Transform. In practise, this eliminates any finite size effect by making the formulation fully periodic. At the same time, the contact problem keeps on being solved in the real space, thus avoiding any aliasing issue. This may affect a fully Fourier-based method when dealing with the pressure peaks typically marking the pressure distributions in viscoelastic contact problems.

Our numerical investigation allows to conclude that the anisotropy tensor of the deformed surface $\mathcal{M}$ can be obtained from the surface anisotropy tensor $\mathbf{M}$ by rotating and stretching the latter. Such an operation can be identified by means of three parameters, that is, the rotation angle φ and the stretching constants σ_1 and σ_2. As a result, this can reduce or increase the solution anisotropy depending on the relative angle between the sliding velocity $\mathbf{v}$ and the surface anisotropy angle α. The crucial point is that the contact solution properties in terms of displacements and contact patches anisotropy cannot be deducted exclusively by looking at the rigid surface. This has to be properly accounted for when coping with, for example, a percolation problem. On the other hand, global contact area and separation are only weakly affected by the surface anisotropy angle α: indeed, in the two elastic limits, i.e., the elastic rubbery regime and the glassy one, nothing can change by changing α, that is, by rotating the surface; in the speed range where viscoelastic effects occurs, we cannot have dramatic deviations with α. Different is the case of the friction force, where the spectral component of the surface in the velocity direction does really matter since it influences the dissipated energy: our results show, for such a reason, a strong dependence on the surface anisotropy. We have a similar trend also in the case of the lateral friction force. This is a component originally shown in this study: it is due to the contact pressure non-symmetric distribution and, although it does not carry out any work and, then, does not dissipate energy, must be

present to guarantee the global equilibrium of the system.

Appendix A. Normal and tangential stresses in sliding viscoelastic contacts

In Appendix A , we discuss on the normal and the tangential stresses originated when sliding a rigid surface over a viscoelastic layer. Once the stresses are known , it will be then straightforward to obtain the two components of the tangential force described in Section 2, i.e., the viscoelastic friction component F_x and the lateral constrain force F_y .

Indeed, if we assume no Coulomb friction, the elementary force $d\mathbf{F}_n$ at the contact interface will be completely along the vector $\mathbf{n}$ being normal to the deformed surface $u(\mathbf{x})$, i.e. $d\mathbf{F}_n = dF_n\mathbf{n}$. Now, let us introduce the unit vectors $\mathbf{k}$, which is normal to the undeformed Cartesian plane Π_0 identified by $\mathbf{i}$ and $\mathbf{j}$, and $\mathbf{e}_\psi$, which is located in Π_0 and defines the direction where the directional derivative $Du(\mathbf{x})$ reaches its maximum value. As well know, such a direction corresponds to that one of the gradient vector $\nabla u(\mathbf{x})$ and, consequently, $\mathbf{e}_\psi$ is equal to $\mathbf{e}_\psi = \nabla u(\mathbf{x}) / |\nabla u(\mathbf{x})|$. We can, then, decompose $d\mathbf{F}_n$ into the normal component $d\mathbf{N}$ along $\mathbf{k}$ and the tangential one $d\mathbf{T}$ along $\mathbf{e}_\psi$:

$$d\mathbf{N} = dN\mathbf{k} = dF_n \cos\beta\mathbf{k} \tag{A.1}$$

$$d\mathbf{T} = dT\mathbf{e}_\psi = dF_n \sin\beta \frac{\nabla u(\mathbf{x})}{|\nabla u(\mathbf{x})|} \tag{A.2}$$

with β being the angle between Π_0 and the plane tangential to the deformed surface $u(\mathbf{x})$. Under the assumption of small displacements, we can linearize Eqs. (A.1) and, in particular, by considering $\cos\beta \approx 1$ and $\sin\beta \approx |\nabla u(\mathbf{x})|$, we can write:

$$d\mathbf{N} = dF_n\mathbf{k} \tag{A.3}$$

$$d\mathbf{T} = dF_n\nabla u(\mathbf{x}) = dN\nabla u(\mathbf{x}) \tag{A.4}$$

Passing from the elementary normal and tangential forces to the normal and tangential stresses can be easily done by dividing the aforementioned expressions for an elementary area dA_0 on the plane Π_0. Thus, we have:

$$\sigma(\mathbf{x}) = \sigma(\mathbf{x})\,\mathbf{k} = \frac{dN}{dA_0}\mathbf{k} = \frac{dF_n}{dA_0}\mathbf{k} \tag{A.5}$$

$$\tau(\mathbf{x}) = \tau(\mathbf{x})\,\mathbf{e}_\psi = \frac{dT}{dA_0}\mathbf{e}_\psi = \sigma(\mathbf{x})\,\nabla u(\mathbf{x}) \tag{A.6}$$

Now, if we project $\tau(\mathbf{x})$ along $\mathbf{i}$ and $\mathbf{j}$, by then integrating over the contact area A, we will obtain respectively the viscoelastic friction component F_x and the lateral constrain force F_y

Appendix B. Numerical generation of anisotropic surfaces

In this Appendix, we briefly report the spectral method employed to generate homogeneous randomly rough surfaces with given anisotropic properties. To this end, first of all, let us introduce the power spectral density $C(\mathbf{q}) = (2\pi)^{-2}\int d^2x\,\langle h(\mathbf{x})\,h(\mathbf{0})\rangle \exp(-i\mathbf{q}\cdot\mathbf{x})$, where $\mathbf{q} = (q_1, q_2)$ is the wave-vector, $h(\mathbf{x})$ refers to the single realization of the surface spatial height distribution, and the symbol $\langle\cdot\rangle$ stands for the statistical average over a very large number of surface realizations, i.e. the so-called ensemble average. To generate the anisotropic surface, we assume the following form for the PSD:

$$C(\mathbf{q}) = C\left(\sqrt{\frac{q_1^2}{a^2} + \frac{q_2^2}{b^2}}\right) \tag{B.1}$$

where a and b are two dimensionless real number chosen in such a way that $a^2 + b^2 = 2$ and $b/a = \varepsilon$ with ε being the PSD eccentricity. Indeed, Equation (B.1) implies that the contours of the PSD are represented by ellipses defined by the relation:

$$\frac{q_1^2}{a^2} + \frac{q_2^2}{b^2} = \rho^2 \tag{B.2}$$

which reduces to the equation of the circle $q_1^2 + q_2^2 = \rho^2$ when $\varepsilon = 1$. Incidentally, let us observe that ρ has the same dimensions as q_1 and q_1, i.e. l^{-1} where l is the dimension of spatial lengths. Now in order to completely define the PSD, we must define the functional form for Eq. (B.1). To this purpose, we choose a surface which appears to be self-affine in a certain range

of frequencies:

$$
\begin{aligned}
C(\mathbf{q}) &= C_0 \left[\frac{1}{q_1^2 + q_2^2} \left(\frac{q_1^2}{a^2} + \frac{q_2^2}{b^2} \right) \right]^{-(H+1)} ; \qquad q_l \leq q \leq q_r \\
C(\mathbf{q}) &= C_0 \left[\frac{1}{q_r^2} \left(\frac{q_1^2}{a^2} + \frac{q_2^2}{b^2} \right) \right]^{-(H+1)} ; \qquad q_r \leq q \leq q_c \\
C(\mathbf{q}) &= 0; \qquad q \geq q_c
\end{aligned}
\tag{B.3}
$$

where $q_l = 2\pi/L$, with L being the lateral size of the surface we need to generate. We also defined $q = |\mathbf{q}|$, and q_r and q_c the roll-off and cut-off wavevector respectively. The quantity H is the so-called Hurst exponent of the surface, related the fractal dimension D_f trough the formula $D_\mathrm{f} = 3 - H$. Note that Eq. (B.2) is a canonical representation of the ellipse. Therefore, Eq. (B.1) represents a randomly rough surface with the two principal directions of anisotropy aligned along the x- and y- axes respectively. The argument of Eq. (B.1) can be equivalently represented in tensorial form as:

$$
\mathbf{T}\mathbf{q} \cdot \mathbf{q} = T_{ij} q_i q_j = \rho^2 \tag{B.4}
$$

where the Einstein summation notation is used. The symmetric tensor $\mathbf{T} \equiv T_{ij}$ has, in this case, a diagonal representation: its components are $T_{11} = a^{-2}$, $T_{12} = T_{21} = 0$, $T_{22} = b^{-2}$.

Now, in order to generate an anticlockwise rotation for the surface principal directions, we need just to rotate the ellipse of an angle α. Thus, let us define the rotation matrix $\mathbf{R}_\alpha$ such that $R_{11} = \cos\alpha$, $R_{12} = -\sin\alpha$, $R_{21} = \sin\alpha$, $R_{22} = \cos\alpha$. Then, we first rotate the tensor $\mathbf{T}$ using the formula:

$$
\mathbf{T}_\alpha = \mathbf{R}_\alpha \mathbf{T} \mathbf{R}_\alpha^\mathbf{T} \tag{B.5}
$$

where $\mathbf{R}_\alpha^T$ is the transpose matrix of $\mathbf{R}_\alpha$. Therefore, we can define the equation of the rotated ellipse as

$$
\mathbf{T}_\alpha \mathbf{q} \cdot \mathbf{q} = \rho^2
$$

It follows that the PSD of the anticlockwise rotated surface becomes $C(\mathbf{q}) = C(\mathbf{T}_\alpha \mathbf{q} \cdot \mathbf{q})$ and, for the self-affine case considered here, we can rewrite Eq.

(B.1) as:

$$\begin{aligned} C(\mathbf{q}) &= C_0 \left(\frac{\mathbf{T}_\alpha \mathbf{q} \cdot \mathbf{q}}{q_1^2 + q_2^2} \right)^{-(H+1)} ; \qquad q_l \leq q \leq q_r \\ C(\mathbf{q}) &= C_0 \left(\frac{\mathbf{T}_\alpha \mathbf{q} \cdot \mathbf{q}}{q_r^2} \right)^{-(H+1)} ; \qquad q_r \leq q \leq q_c \\ C(\mathbf{q}) &= 0; \qquad q \geq q_c \end{aligned} \tag{B.6}$$

Now, it is straightforward to generate the surface with a certain degree of anisotropy by using a spectral approach and the Fast Fourier Transform (FFT) technique.

To this end, we generate a periodic surface whose representation in exponential form is:

$$h(\mathbf{x}) = \sum_{k,h=-\infty}^{+\infty} a_{hk} e^{i \mathbf{q}_{kh} \cdot \mathbf{x}} \tag{B.7}$$

where a_{hk} are random complex numbers, $\mathbf{q}_{kh} = (kq_l, hq_l)$, $\mathbf{x} = (x, y)$. Since $h(\mathbf{x})$ is real, we must have $a_{-h,-k} = \overline{a_{hk}}$. Moreover, for randomly rough surface, the following relation must be satisfied: $\langle a_{hk} a_{lm} \rangle = 0$ with $l \neq -h,\ m \neq -k$. For such a surface, the PSD is equal to:

$$C(\mathbf{q}) = \sum_{k,h=-\infty}^{+\infty} \left\langle |a_{hk}|^2 \right\rangle \delta(\mathbf{q} - \mathbf{q}_{hk}) \tag{B.8}$$

from which it follows:

$$C(\mathbf{q}_{hk}) = \left\langle |a_{hk}|^2 \right\rangle \delta(\mathbf{0}) \tag{B.9}$$

using that the value of $\delta(\mathbf{0})$ in discrete terms, i.e. $\delta(\mathbf{0}) = q_L^{-2} = L^2/(4\pi^2)$, we obtain:

$$\left\langle |a_{hk}|^2 \right\rangle = \left(\frac{2\pi}{L} \right)^2 C(\mathbf{q}_{hk}) \tag{B.10}$$

In order to completely characterize the rough surface, we still need the probability distribution of the quantities a_{hk}. Thus, let us write a_{hk} as $a_{hk} = \alpha_{hk} + i\beta_{hk}$ where α_{hk} and β_{hk} are independent random real variables. Note that the condition $a_{-h,-k} = \overline{a_{hk}}$ yields $\alpha_{-h,-k} = \alpha_{hk}$ and $\beta_{-h,-k} = -\beta_{hk}$. In order to generate a random Gaussian surface, α_{hk} and β_{hk} must follow a Gaussian distribution with zero mean, i.e. $\langle \alpha_{hk} \rangle = \langle \beta_{hk} \rangle = 0$ and same variance $\langle \alpha_{hk}^2 \rangle = \langle \beta_{hk}^2 \rangle = \sigma_{hk}^2$. Note that this choice fulfill the

condition $\langle a_{hk} a_{lm} \rangle = 0$ with $l \neq -h$, $m \neq -k$. Now, observing that $\left\langle |a_{hk}|^2 \right\rangle = \langle \alpha_{hk}^2 \rangle + \langle \beta_{hk}^2 \rangle = 2\sigma_{hk}^2$, and using Eq. (B.10) one obtains

$$\sigma_{hk}^2 = \frac{1}{2} \left(\frac{2\pi}{L} \right)^2 C\left(\mathbf{q}_{hk}\right) \tag{B.11}$$

Therefore in order to generate the randomly rough anisotropic surface, first of all, we have to drawn the values of α_{hk} and β_{hk} from two identical Gaussian distribution of zero mean and variance given by Eq. (B.11), calculate the quantity $a_{hk} = \alpha_{hk} + i\beta_{hk}$, and then use the FFT procedure to compute Eq.(B.7).

[1] Thatte A., Salant R. F., Effects of multi-scale viscoelasticity of polymers on high-pressure, high-frequency sealing dynamics, Tribology International, 52, 75–86, (2012).

[2] Shukla A. and Datta T. , Optimal Use of Viscoelastic Dampers in Building Frames for Seismic Force. Journal of Structural Engineering, 125 (4), 401–409, (1999).

[3] Takewaki I. Building Control with Passive Dampers: Optimal Performance-based Design for Earthquakes, John Wiley & Sons, (2011).

[4] Geim, A.K., Dubonos, S.V., Gricorieva, I.V., Novoselov, K.S., Zhukov, A.A., Shapoval, S.Yu., Microfabricated adhesive mimicking gecko foothair. Nat. Mater. 2, 461–463, (2003).

[5] Dening, K., Heepe, L., Afferrante, L., Carbone G., Gorb S., Adhesion control by inflation: Implications from biology to artificial attachment device, Applied Physics A: Materials Science and Processing, 116(2), 567-573, (2014).

[6] Arzt E. , Gorb S., and Spolenak R., From micro to nano contacts in biological attachment devices. Proceedings of the National Academy of Sciences, 16, 100 , 19 , 10603–10606, (2003).

[7] Lin S. , Ryu S. , Tokareva O., Gronau G., Jakobsen M.M.,Huang W. , Rizzo D.J., Li D.,Stai C. ,Pugno N. , Wong J.Y.,Kaplan D.L. , Buehler M.J.. Predictive modelling-based design and experiments for synthesis and spinning of bioinspired silk fibres. Nature Communication 6, 6892, (2015).

[8] Angelini T. E. , Dunn A. C., Uruena J. M., Dickrell D. J., Burris D. L. and Sawyer W. G. , Cell Friction, Faraday Discussion , 156, 31–39, (2012).

[9] Dunn A. C., Cobb J. A., Kantzios A. N., Lee S. J. , Sarntinoranont M. , Tran-Son-Tay R. , Sawyer W. G. , Friction Coefficient Measurement of Hydrogel Materials on Living Epithelial Cells, Tribology Letters, 30, 1,13-19, (2008).

[10] Chortos A, Liu J, Bao Z., Pursuing prosthetic electronic skin, Nature, 15,937,2016.

[11] J. A. Greenwood and J. B. P. Williamson, Contact of Nominally Flat Surfaces, Proceedings of Royal Society London A, 295 (1442), 300-319 (1966)

[12] Greenwood, J.A., Putignano, C., Ciavarella, M. A Greenwood & Williamson theory for line contact. Wear. 270, 332-334,(2011).

[13] Bush A.W. ,Gibson R.D. ,Thomas T.R. . The elastic contact of a rough surface, Wear, 35,87-111, (1975).

[14] Carbone G. , Bottiglione F., Asperity contact theories: Do they predict linearity between contact area and load?, Journal of the Mechanics and Physics of Solids 56 2555-2572, (2008).

[15] Afferrante, L., Carbone, G., Demelio G., Interacting and coalescing Hertzian asperities: A new multiasperity contact model, Wear, 278-279, 28-33, (2012).

[16] Afferrante, L., Bottiglione, F., Putignano, C., Persson, B.N.J., Carbone, G. (2018). Elastic contact mechanics of randomly rough surfaces: an assessment of advanced asperity models and Persson's theory. Tribology Letters. 66(2), 75, (2018).

[17] Persson B.N.J., Theory of rubber friction and contact mechanics, Journal of Chemical Physics, 115, 3840 -3861, (2001).

[18] Carbone G., Scaraggi M., Tartaglino U., Adhesive contact of rough surfaces: comparison between numerical calculations and analytical theories", The European Physiscal Journal E – Soft Matter, **30** (1), 65-74, (2009).

[19] Putignano C., Afferrante L. , Carbone G., Demelio G. , The influence of the statistical properties of self-affine surfaces in elastic contact: a numerical investigation, Journal of Mechanics and Physics of Solids, 60, 5, 973–982, (2012).

[20] Putignano C., Afferrante L., Carbone G., Demelio G. A new efficient numerical method for contact mechanics of rough surfaces. International Journal of Solids and Structures, 49 (2), 338-343, (2012).

[21] Paggi M., Ciaveralla M., The coefficient of proportionality k between real contact area and load, with new asperity models, Wear 268 1020–1029 (2010).

[22] V. A. Yastrebov, G. Anciaux, and J. F. Molinari, Contact between representative rough surfaces. Phys. Rev. E 86, 035601(R), (2012).

[23] V.A. Yastrebov, G. Anciaux, J.F. Molinari. "The role of the roughness spectral breadth in elastic contact of rough surfaces". Journal of the Mechanics and Physics of Solids, 107:469-493 (2017).

[24] Ju Y.and Farris T. N. , Spectral Analysis of Two-Dimensional Contact Problems, J. Tribol 118(2), 320-328, 1996.

[25] Stanley H. M. and Kato T., An FFT-Based Method for Rough Surface Contact, J. Tribol 119(3), 481-485, 1997.

[26] Campana, C, Muser, M.H., Contact Mechanics of Real vs Randomly Rough Surfaces: A Green's Function Molecular Dynamics Study, Europhys. Lett. 77 (3), 38005,2007..

[27] Dapp, W.B., Lücke, A., Persson, B.N.J., Müser, M.H., Self-affine elastic contacts: Percolation and leakage, Physical Review Letters, 108 (24), 244301, (2012).

[28] Sahlia R., Pallares G., Ducottet C., Ben Alid I. E. , Al Akhrassd S., Guiberta M. , and Scheibert J. , Evolution of real contact area under shear and the value of static friction of soft materials, PNAS,115, 471–476, (2017).

[29] Bao G. , Suresh S., Cell and molecular mechanics of biological materials, Nature Materials 2, 715 - 725, (2003).

[30] Hunter S.C. , The rolling contact of a rigid cylinder with a viscoelastic half space . Trans. ASME, Ser. E, J. Appl. Mech. 28, 611–617 (1961).

[31] Carbone G. , Putignano C., A novel methodology to predict sliding/rolling friction in viscoelastic materials: theory and experiments., Journal of Mechanics and Physics of Solids, Journal of the Mechanics and Physics of Solids, 61 (8), 1822-1834, (2013).

[32] Menga N , Afferrante L ,Carbone G , Effect of thickness and boundary conditions on the behavior of viscoelastic layers in sliding contact with wavy profiles Journal of the Mechanics and Physics of Solids 95, 517-529 .

[33] Grosch K. A. , The Relation between the Friction and Visco-Elastic Properties of Rubber, Proceedings of the Royal Society of London. Series A, Mathematical and Physical, 274-1356, 21-39, (1963).

[34] Putignano C., Reddyhoff T., Carbone G., Dini D., Experimental investigation of viscoelastic rolling contacts: a comparison with theory. Tribology Letters , 51, 105–113, (2013).

[35] Putignano C. , Reddyhoff T. , Dini D. . The influence of temperature on viscoelastic friction properties. Tribology International, 100, 338-343, (2016).

[36] Kusche S., Frictional force between a rotationally symmetric indenter and a viscoelastic half-space, Journal of Applied Mathematics and Mechanics , 97,2, 226â€“239, (2017).

[37] Carbone G. , Putignano C. . Rough viscoelastic sliding contact: theory and experiments. Physical Review E, 89, 032408, (2014).

[38] Koumi K. E., Chaise T., Nelias D., Rolling contact of a rigid sphere/sliding of a spherical indenter upon a viscoelastic half-space containing an ellipsoidal inhomogeneity, Journal of the Mechanics and Physics of Solids, 80, 1–25, (2015).

[39] Koumi KE,Nelias D ,Chaise T , Duval A, Modeling of the contact between a rigid indenter and a heterogeneous viscoelastic material, Mechanics of Materials 77, 28-42, (2014).

[40] Putignano C. , Carbone G. , Dini D., Mechanics of Rough Contacts in Elastic and Viscoelastic Thin Layers, International Journal of Solids and Structures, 69–70, 507–517, (2015).

[41] Putignano C. , Carbone G., Dini D. , Theory of reciprocating contact for viscoelastic solids. Physycal Review E 93, 043003, (2016).

[42] Putignano C., Carbone G. Viscoelastic Damping in alternate reciprocating contacts,Scientific Reports 7 (2017).

[43] Putignano C., Carbone G. , Viscoelastic reciprocating contacts in presence of finite rough interfaces: a numerical investigation. Journal of the Mechanics and Physics of Solids, 114, 185-193, (2018).

[44] Christensen R. M., Theory of viscoelasticity, Academic Press, New York, (1982).

[45] Williams M.L., Landel R.F. , Ferry J.D. ,The Temperature Dependence of Relaxation Mechanisms in Amorphous Polymers and Other Glass-forming Liquids, J. Amer. Chem. Soc., 77:3701, (1955).

[46] Johnson, K.L.J., Contact Mechanics, Cambridge University Press, (1985).

[47] Longuet-Higgins M. S. , The statistical analysis of a random, moving surface, Phil. Trans. R. Soc. London A 249, 321 (1957).

[48] Putignano C., Dini D. , Soft matter lubrication: does solid viscoelasticity matter?, ACS Applied Materials & Interfaces, 9 (48), 42287-42295, (2017).

[49] Putignano C. , Carbone G., Viscoelastic reciprocating contacts in presence of finite rough interfaces: a numerical investigation. Journal of the Mechanics and Physics of Solids, 114, 185-193, (2018).

[50] Bottiglione F. , Carbone G. , Mangialardi L. , Mantriota G. , Leakage mechanism in flat seals, J. Appl. Phys. 106, 104902 (2009).

[51] Lorenz B. and Persson B.N.J., Leak rate of seals: Effective-medium theory and comparison with experiment, Eur. Phys. J. E 31, 159–167 (2010) .

[52] Dapp W. B. & Müser M. H. , Fluid leakage near the percolation threshold, Scientific Reports, 6, 19513 (2016).

[53] Vladescu S., Putignano C. , Marx N. , Keppens T., Reddyhoff T. , Dini D., The percolation of liquid through a compliant seal - an experimental and theoretical study, Journal of Fluids Engineering, 141(3), 031101, (2019).

[54] Putignano C. , Viscoelastic rough contact mechanics: a multiscale investigation, Journal of Mechanical Engineering Science, Proceedings of the Institution of Mechanical Engineers, Part C: Journal of Mechanical Engineering Science, 0954406216631005, (2016).